Electronic Supplementary Material (ESI) for Nanoscale.

Supplementary Information For Gate Tunable WSe_2-BP van der Waals Heterojunction Devices

Peng Chen[1], Ting Ting Zhang[1], Jing zhang[1], Jianyong Xiang[2], Hua Yu[1], Shuang Wu[1], Xiaobo Lu[1], Guole Wang[1], Fusheng Wen[2], Zhongyuan Liu[2], Rong Yang[1], Dongxia Shi[1] & Guangyu Zhang[1,3,*]

[1] *Beijing National Laboratory for Condensed Matter Physics and Institute of Physics, Chinese Academy of Sciences, Beijing 100190, China*

[2] *State Key Laboratory for Metastable Materials Science and Technology, Yanshan University, Qinhuangdao 066004, China*

[3] *Collaborative Innovation Center of Quantum Matter, Beijing 100190, China*

* Corresponding author. **Email:** gyzhang@iphy.ac.cn

Main Contents

F. Band alignment of p-p junction at different bias

G. The spatially resolved photocurrent measurement

H. The electrical performance of other device

I. References

A. Device Fabrication Procedure

WSe_2 and BP layers were exfoliated using scotch tape method[1]. The WSe_2 flake was exfoliated on a Si/SiO_2 substrate (100 nm SiO_2) whereas BP flake was exfoliated on a PVA (polyvinyl alcohol)/PMMA bilayer[2]. Then, we transferred the bilayer film from substrate with a perforated scotch tape, and the film was suspended on the hole of scotch tape. The BP flake was then transferred onto the desired location on the WSe_2 layer, using a modified high resolution microscope system. The substrate was heated to 60 ℃ during the transfer process. The PVA and PMMA polymer were removed by the deionized water and Acetone. Finally, the heterojunction devices with Ti/Au (6 nm/50 nm) electrodes were fabricated using standard electron-beam lithography followed by metal evaporation and lift-off.

B. AFM characterization of the BP-WSe_2 heterojunction

The surface morphology of the heterojunction has been characterized by an atomic force microscope (AFM) operated in the tapping mode (Figure S1). The thickness of WSe_2 and BP is 12 nm and 20 nm, respectively. There are some bubbles presents in our sample. The bubbles generated during the transfer process.

C. Raman Spectra of the main device

Figure S2 shows the Raman spectrum of BP (black curve), WSe_2 (red curve) and WSe_2/BP heterostructure (blue curve). Raman peaks of BP at 362 cm^{-1}, 439 cm^{-1}, and 467 cm^{-1} are attributed to the A_g^1, B_g^2, and A_g^2 phonon modes, respectively[3]. Raman peaks of WSe_2 at 249 cm^{-1}, 258 cm^{-1} are attributed to the E_{2g}^1 and A_{1g} phonon modes. The peak at 308 cm^{-1} may origin from the interlayer interaction. The other peaks observed in the range of 100-450 cm^{-1} are assigned as the second order and combinational modes[4]. Raman peaks of the overlapped region consist of contributions from both WSe_2 and BP with a slight shift, indicating a good quality of this van der Waals heterojunction.

D. Semi-log plot of I_{DS}-V_{DS} curves in Figure 2a of the main text

Figure S3 shows the I_{DS}-V_{DS} curves for the p-p junction in semi-log scale. The reversed current is about 10^{-11} A at V_{DS}=-3V.

E. Exclude the influence of contact resistance

The I_{DS}-V_{DS} measurements of D1-D2 and S1-S2 were shown in Fig. S4. From the data, we could see the I_{DS}-V_{DS} curve of BP is linear, while the I_{DS}-V_{DS} curve of WSe_2 is nonlinear at V_{BG}=-30 V. These results indicate the contact of BP (p-type) is ohmic, while the contact of WSe_2 (p type) is Schottky contact. As the Schottky diode could also lead to the current rectification, we carefully analyzed the influence of Ti/WSe_2 Schottky barrier to the current rectification observed in p-p junction.

Firstly, we evaluated the contribution of contact with the help of the band alignment of Ti and WSe_2. Fig.S5 shows the band alignment of Ti and p type-WSe_2, where a Schottky barrier Φ_s is present at the interface. When V>0, the holes will transport from metal to WSe_2, and need to overcome the Schottky barrier Φ_s. When V<0, the holes will transport from WSe_2 to metal, and don't need to overcome the barrier Φ_s. It means the contact resistance of Ti/WSe_2 at V>0 is larger than that at V<0. This is obviously discrepancy with the experimental result, indicating the contact plays a trivial role in the heterojunction device.

Secondly, we compared the contact resistance and junction resistance. From the I_{DS}-V_{DS} measurement of D1-D2, we obtained the device resistance R1< 8 MΩ at V_{BG}=-30 V. R1 contain two parts: the sheet resistance of WSe_2 and the contact resistance of Ti/WSe_2. Thus, either the contact resistance or sheet resistance of WSe_2 should be smaller than 8 MΩ (V_{BG}=-30 V). From the D1-S1 measurement, we found R2~100 GΩ at V=-3 V (calculated from Fig. S3), and it is 10^4 times larger than R1. R2 contains three parts: the sheet resistance of WSe_2 and BP, the contact resistance of WSe_2 and BP and the junction resistance of WSe_2/BP. Such a large R2 can't be attributed to the contact resistance or sheet resistance, and can be only attributed to the junction resistance.

F. Band alignment of p-p junction at different bias

The band alignments of WSe_2-BP p-p junction at different bias were illustrated at Figure S6. With $V_{DS}<0$, the holes transport from BP to WSe_2, and a large energy barrier ΔE_v presents at interface. With $V_{DS}>0$, the holes transport from WSe_2 to BP, and a small energy barrier presents at interface.

G. The spatially resolved photocurrent measurement

To further confirm the photocurrent is generated from the junction, the spatially resolved photocurrent measurement was carried out (Figure S7). The wavelength of the incident laser is 785 nm. The power of the laser is 12.5μw, and the spot size of the laser is about 1 um. The device was tuned to p-p junction with applying V_{BG}=-20 V, and the current was measured under 0 V bias. We could see that the photocurrent is almost generated at the junction area.

H. The electrical performance of other device

Figure S8a and S85b show the optical image and AFM image of another heterojunction. The thickness of WSe_2 and BP is 7 nm and 18 nm, respectively. We observed similar electircal performance in this device, where the p-p junction show large current rectification ratio, and the n-n junction show neglect current rectification ratio (Figure S8c and Figure S8d).

I. References:

1. Novoselov, K. S.; Geim, A. K.; Morozov, S. V.; Jiang, D.; Zhang, Y.; Dubonos, S. V.; Grigorieva, I. V.; Firsov, A. A. *Science* **2004,** 306, (5696), 666-669.
2. Lee, C. H.; Lee, G. H.; van der Zande, A. M.; Chen, W. C.; Li, Y. L.; Han, M. Y.; Cui, X.; Arefe, G.; Nuckolls, C.; Heinz, T. F.; Guo, J.; Hone, J.; Kim, P. *Nat. Nanotechnol.* **2014,** 9, (9), 676-681.
3. Liu, H.; Neal, A. T.; Zhu, Z.; Luo, Z.; Xu, X.; Tománek, D.; Ye, P. D. *ACS Nano* **2014,** 8, (4), 4033-4041.
4. Li, H.; Lu, G.; Wang, Y.; Yin, Z.; Cong, C.; He, Q.; Wang, L.; Ding, F.; Yu, T.; Zhang, H. *Small* **2013,** 9, (11), 1974-1981.

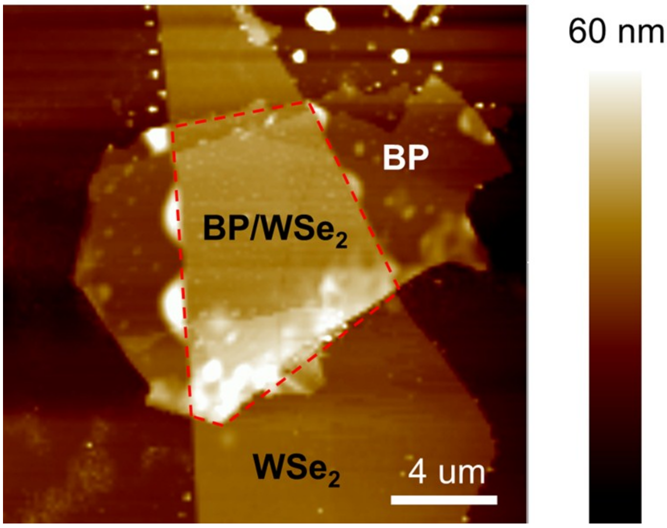

Figure S1. AFM image of the WSe_2-BP heterostructure. The red dashed line denotes the boundary of overlapped region.

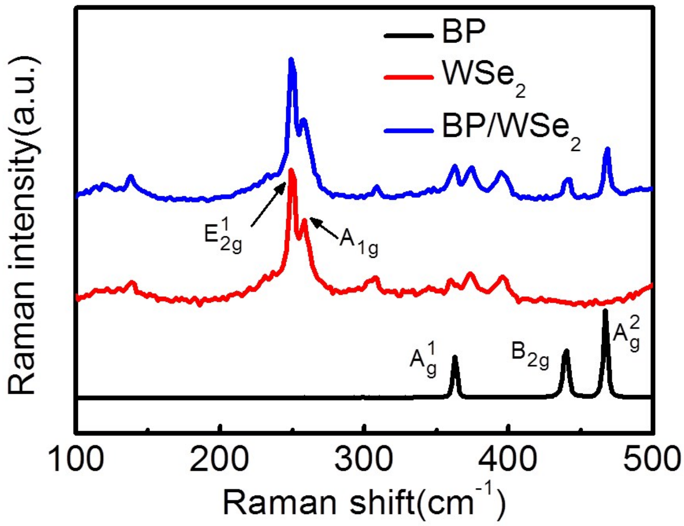

Figure S2. Raman Spectrum of the main device. The black, red and blue curve denotes the Raman spectrum of BP, WSe_2, WSe_2/BP, respectively.

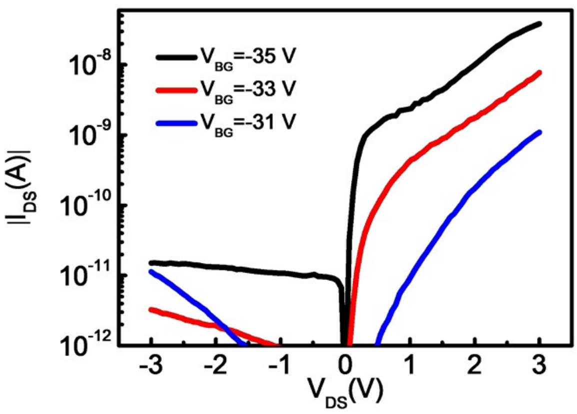

Figure S3. The semi-log plot of Semi-log plot of I_{DS}-V_{DS} curves in Figure 2a of the main text.

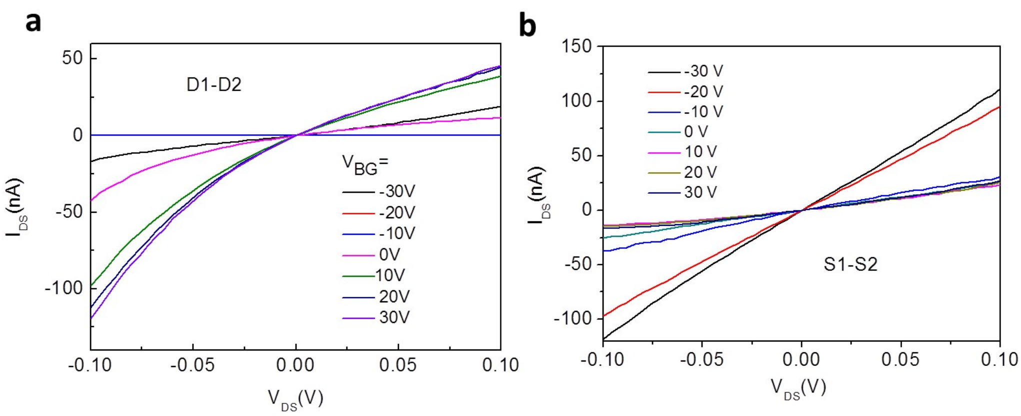

Figure S4. (a) The I_{DS}-V_{DS} curves of D1-D2. (b) The I_{DS}-V_{DS} curves of S1-S2.

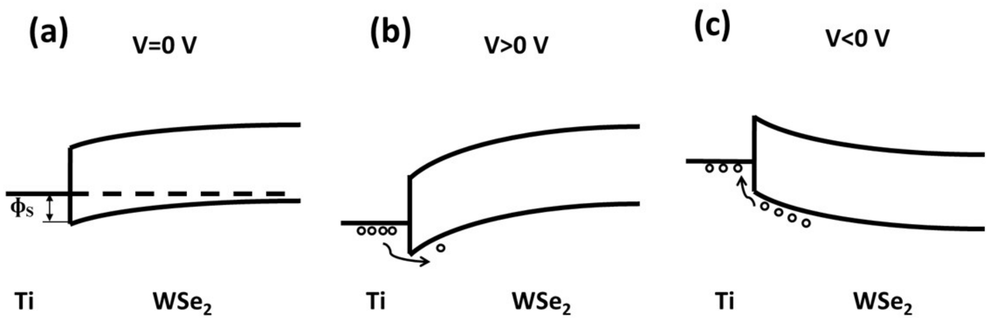

Figure S5. The band alignment of Ti-WSe_2(p-type) at V=0 (a), V>0 (b) and V<0 (c).The open black circles denote holes in valence band. The black arrow denotes the moving direction of holes.

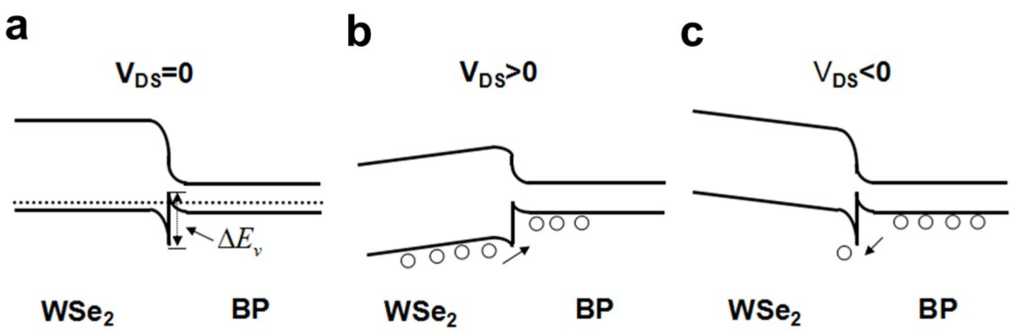

Figure S6. The band alignment of p-p junction at V_{DS}=0 (a), V_{DS}>0 (b) and V_{DS}<0 (c).The open black circles denote holes in valence band. The black arrow denotes the moving direction of holes.

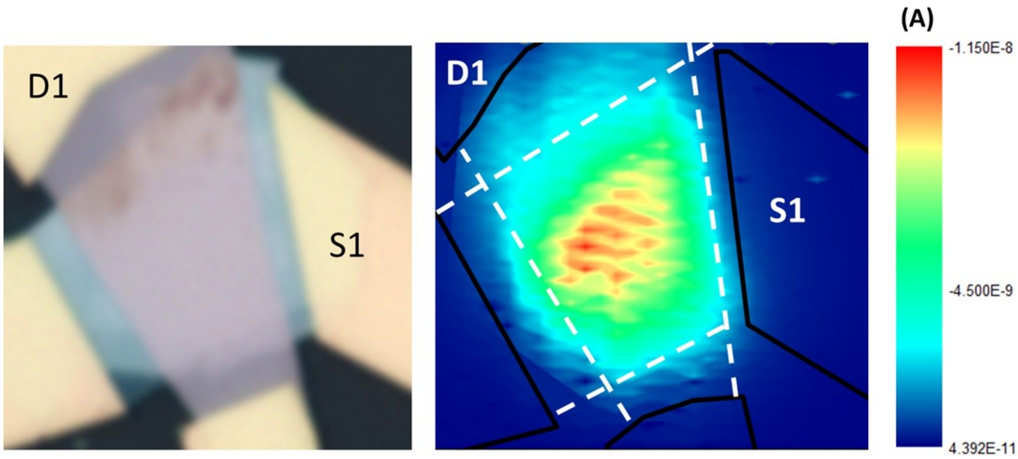

Figure S7. Spatially resolved photocurrent measurement of the WSe_2-BP heterojunction device.

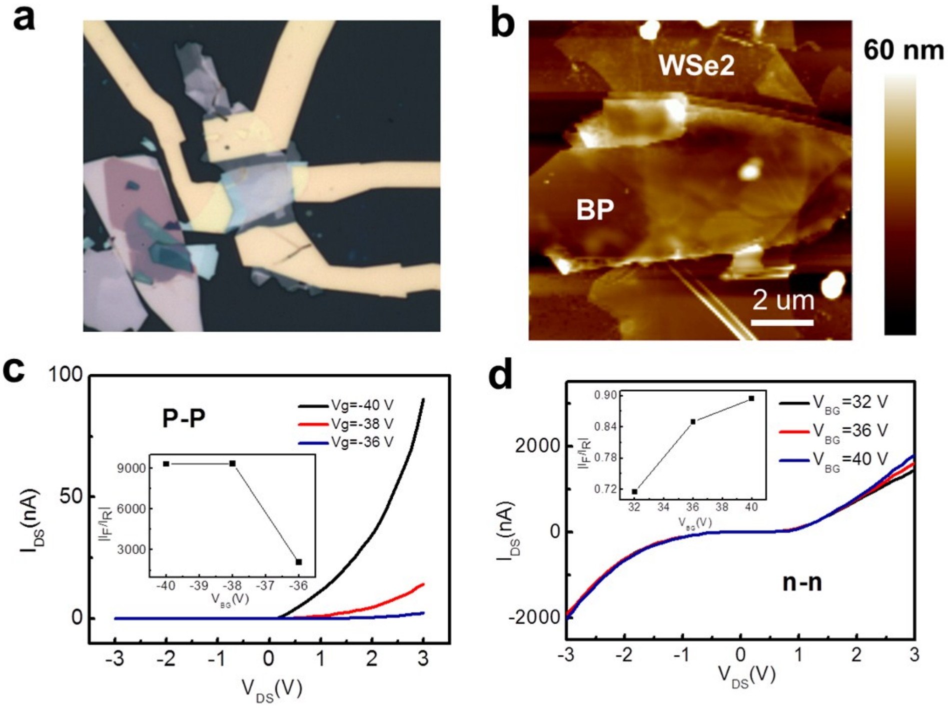

Figure S8. (a) Optical image of WSe_2-BP heterojunction device. (b) AFM image of the device shown in (a). (c) The I_{DS}-V_{DS} curves of p-p junction. Inset shows the $|I_F/I_R|$ at V_{BG}=-40 V, -38 V and -36 V. (d) The I_{DS}-V_{DS} curves of n-n junction. Inset shows the $|I_F/I_R|$ at V_{BG}=32 V, 36 V and 40 V. Inset shows the $|I_F/I_R|$ at V_{BG}=32 V, 36 V and 40 V.